Performance evaluation of a multiscale modelling system applied to particulate matter dispersion in a real traffic hot spot in Madrid (Spain)

J.L. Santiago[a,*], B. Sanchez[e,a], C. Quaassdorff[b], D. de la Paz[b], A. Martilli[a], F. Martín[a], R. Borge[b], E. Rivas[a], F.J. Gómez-Moreno[a], E. Díaz[a], B. Artiñano[a], C. Yagüe[c], S. Vardoulakis[d]

[a] *Atmospheric Pollution Division, Environmental Department, CIEMAT, Spain*
[b] *Laboratory of Environmental Modelling, Universidad Politécnica de Madrid (UPM), Madrid, Spain*
[c] *Department of Earth Physics and Astrophysics, Universidad Complutense de Madrid (UCM), Faculty of Physical Sciences, Spain*
[d] *National Centre for Epidemiology and Population Health, Research School of Population Health, Australian National University, Canberra, Australia*
[e] *Department of Geography, National University of Singapore, Singapore*

A B S T R A C T

Urban air pollution is one of the most important environmental problems nowadays. Understanding urban pollution is rather challenging due to different factors that produce a strongly heterogeneous pollutant dis- tribution within streets. Observed concentrations depend on processes occurring at a wide range of spatial and temporal scales, complex wind flow and turbulence patterns induced by urban obstacles and irregular traffic emissions. The main objective of this paper is to model particulate matter dispersion at microscale while con- sidering the effects of mesoscale processes. Computational Fluid Dynamic (CFD) PM_{10} simulations were per- formed taking into account high spatial resolution traffic emissions from a microscale traffic model and inlet vertical profiles of meteorological variables from Weather Research and Forecasting (WRF) model. This mod- elling system is evaluated by using meteorological and PM_{10} concentration data from intensive experimental campaigns carried out on 25th February and 6th July, 2015 in a real urban traffic hot-spot in Madrid. The effect of uncertainties in the inlet profiles from mesoscale input data on microscale results is assessed. Additionally, the importance of the sensible surface heat fluxes (SHF) provided by WRF and the selection of an appropriate turbulent Schmidt number in the dispersion equation are investigated. The main conclusion is that the modelling system accurately reproduces PM_{10} dispersion imposing appropriate inputs (meteorological variables and SHF) and a suitable turbulent Schmidt number. Better agreement is found for simulation with a low turbulent Schmidt number. This approach improves the standard microscale modelling alone because more realistic boundary conditions and mesoscale processes are considered.

Keywords: Computational fluid dynamic (CFD) modelling; Microscale traffic emissions; Multiscale modelling $PM_{10;}$ Turbulent schmidt number; Weather research and forecasting (WRF) model

1. Introduction

Urban air quality is one of the most important environmental challenges and a public concern due to the impact of air pollution on human health. More than 50% of world population (and more 70% of European population) lives in cities and, therefore, is exposed to high pollution levels (EEA 2015; WHO 2018; EEA 2018).

The interaction of the atmosphere with urban obstacles induces complex flow patterns within the urban canopy that modifies pollution dispersion patterns. This fact besides the irregular traffic emissions along the roads in a city gives rise to a heterogeneous pollutant dis- tribution within and around streets. Hence these strong concentration gradients can only be simulated by high spatial resolution modelling.

For this reason, computational fluid dynamics (CFD) models have the potential to be an adequate tool to analyze this issue because they can resolve explicitly the complex air flow and dispersion induced by urban obstacles (Vardoulakis et al., 2003, 2011). Despite their complexity, the increase of computational resources has made possible their application to real complex urban environments (Buccolieri et al., 2011; Amorim et al., 2013; Jeanjean et al., 2017; Santiago et al., 2017a; Sanchez et al., 2017; Rivas et al., 2019). On the other hand, pollution levels within the city depends on a wide range of atmospheric spatial and temporal scales from the continental to the street scale (Britter and Hanna, 2003). Therefore, all of these scales should be considered in simulations of urban air quality. Moreover, recent work of Arrillaga et al. (2018) have shown the importance of the interactions between mesoscale and

Peer review under responsibility of Turkish National Committee for Air Pollution Research and Control.
* Corresponding author.
E-mail address: jl.santiago@ciemat.es (J.L. Santiago).

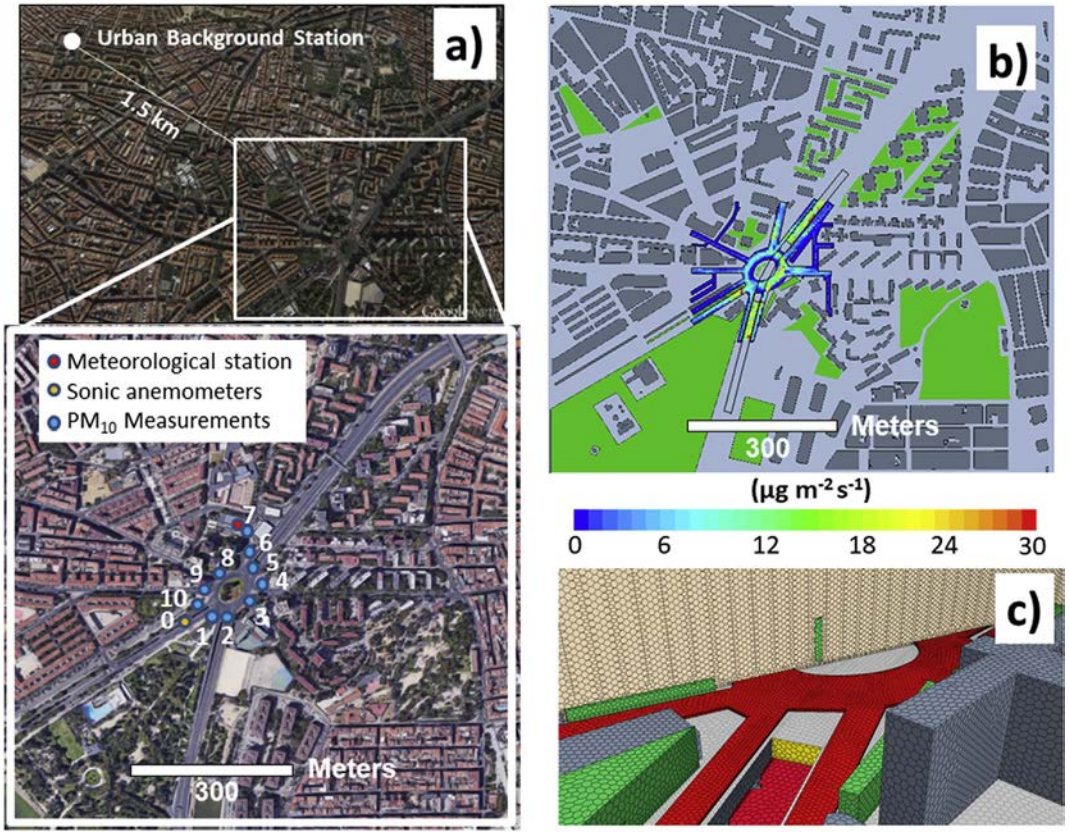

Fig. 1. a) Study area with the location of measurements. b) Central area of the numerical domain including 1 $p.m._{10}$ traffic emission scenario and the simulated vegetation (in green). c) Mesh details.

microscale meteorology, for example between thermally-driven flows and the dynamics of the atmospheric boundary layer (ABL) that can have an important effects on the dispersion of pollutants. Neutral inlet profiles of velocity, turbulent kinetic energy and its dissipation defined by Richards and Hoxey (1993) were widely used in CFD simulations (Buccolieri et al., 2011; Santiago et al., 2013; Jeanjean et al., 2017; Rivas et al., 2019) taking into account wind speed and direction re- corded in nearby meteorological stations. However, to consider all scales processes described above in CFD simulations seems to be ne- cessary accounting for outputs from mesoscale models. Recent studies on the coupling of mesoscale models with CFD models, indicated that this is still a technically challenging approach. A variety of techniques has been investigated: Baik et al. (2009) used vertical profiles of wind speed, turbulent kinetic energy and its dissipation rate from MM5 as input boundary conditions for CFD simulations; Kwak et al. (2015) and Borge et al. (2018) also included the temperature from the Weather Research and Forecasting (WRF) mesoscale model, to provide CFD boundary conditions; additionally, Kwak et al. (2015) imposed a 2-m air temperature from mesoscale model in the CFD simulation. These studies indicate that the exchange of variables between meso and microscale should be analyzed in detail, as well as how to incorporate in the microscale model features modelled only in the mesoscale model, like thermal effects. Several CFD studies showed thermal effects can change wind flow and pollutant dispersion within street canyons. Some of them (Sini et al., 1996; Xie et al., 2007; Cai, 2012) studied simplified heating scenarios considering uniformly heated walls and found changes on wind flow and dispersion within two-dimensional street canyons. In other studies (Qu et al., 2012; Yaghoobian and Kleissl, 2012; Santiago et al., 2014; Nazarian et al., 2018), more realistic urban heating was simulated. Even in recent studies (Toparlar et al., 2015, 2017; Antoniou et al., 2019), urban microclimate is simulated by CFD in real urban locations but not coupling microscale and mesoscale models. However, in this study, to account for thermal effects in a simple way avoiding the extra computational burden of a solar radiation model, sensible surface heat fluxes computed by WRF is used in CFD simulations. On the other hand, detailed traffic emissions are needed to appropriately model urban pollution concentrations by means of CFD techniques. Current developments of microscale traffic emission models allow providing pollutant emissions data with high spatial resolution. These models take into account the effects of traffic lights and the driver behavior (Smit et al., 2007; Quaassdorff et al., 2016) and have been successfully implemented in CFD simulations to compute NO_X dispersion (Sanchez et al., 2017).

The main objective of this paper is to test if a modelling chain composed by a mesoscale model, a microscale CFD model and a microscale traffic emission model can reproduce the high spatial resolution distribution and the time evolution of particulate matter (in this case, PM_{10}) concentration in a real traffic hot spot.

The link between the models is as follows:

- Hourly meteorological variables from mesoscale WRF model (sec- tion 3.1) provide boundary conditions (vertical profiles of wind speed and direction, turbulence) to the CFD microscale simulations.
- Hourly PM_{10} road traffic emissions (exhaust and non-exhaust emissions) from a microscale traffic emission model (Section 3.2) provide emissions to the CFD microscale simulations.
- The closest urban background air quality monitoring station to the study zone (section 3) provides hourly background pollutant concentrations used by the CFD.

This multiscale modelling chain is applied to a real urban hot-spot in Madrid (Spain) where experimental data of meteorological variables, including turbulent kinetic energy, and PM_{10} concentration in several points of the study zone (see Section 2) were recorded in several

experimental campaigns within the framework of TECNAIRE-CM research project (Borge et al., 2016). In this way, the modelling system is evaluated in detail, in order to allow the identification of the main sources of uncertainties in CFD results and the sensitivity of the results to the input variables provided by the mesoscale model (e.g. sensible surface heat fluxes, usually neglected in CFD simulations, or Schmidt number). Note that the meaning of Schmidt number and the influence on pollutant dispersion is described in Section 3.3.

2. Description of the study area and the available experimental data

The area of study is a representative urban hot-spot located in the South-West of Madrid city (Spain). The location is a heavily trafficked roundabout (Plaza Elíptica square) with a main road crossing under it through a tunnel (Fig. 1). The interest to study this zone is mainly due to the high levels of pollution commonly recorded here, where many pedestrian are exposed. The air quality monitoring station usually measured the highest levels of NO_2 concentration in Madrid. For ex- ample, here, in 2015 (the year of this study), it was exceeded the NO_2 annual (40 μg m^{-3}) and hourly limit values (more than 18 h with concentrations over 200 μg m^{-3}) imposed by European air quality Directive. Additionally, this location is complex in terms of urban morphology (different types of buildings and vegetation), intense road traffic flows and the presence of several bus stops and a public transport transfer station (Borge et al., 2016).

Different experiments were carried out in this location in the framework of TECNAIRE-CM research project. This study focuses on one day in winter (25th February) and one day in summer (6th July, 2015) where meteorological variables and PM_{10} measurements at several hours in different points of the square (Fig. 1a) were available to evaluate modelling system performance. Meteorological variables were recorded at three different locations:

- A meteorological station located for these experimental campaigns on a building roof at 18 m above ground level (AGL) recorded wind velocity, air temperature, relative humidity, atmospheric pressure, precipitation and global (incoming) solar radiation. (red point in Fig. 1a). For this study, we focus on wind speed and direction. In the study area, this point is representative of meteorological conditions above the street level.
- Two sonic anemometers recorded the three components of velocity and the temperature with a high sampling frequency (20 Hz) at 6 m and 8 m AGL (orange point in Fig. 1a). From these measurements horizontal wind speed, turbulent kinetic energy (*TKE*) and friction velocity (u_*) were computed. *TKE* and u_* were calculated considering 5-min averages for the evaluation of variance and covariance of wind velocity and using the following equations:

$$TKE = \frac{1}{2}(\overline{u'^2} + \overline{v'^2} + \overline{w'^2}) \quad (1)$$

$$u_* = \sqrt[4]{(\overline{u'w'})^2 + (\overline{v'w'})^2} \quad (2)$$

where u', v' and w' are the turbulent perturbations of the wind components and $u'w'$ and $v'w'$ are the turbulent momentum fluxes (Reynolds stresses). Farther detail of the turbulent parameter evaluation can be found in Borge et al. (2016).

PM_{10} concentration was measured in several locations:

- An Optical Particle Counter Grimm 1107 (Grimm and Eatough, 2009) instrument was deployed at the same location of the lower sonic anemometer.
- A portable TSI DustTrakTM DRX (Tasic et al., 2012) was used to provide ambient air PM_{10} concentrations at 1.5 m AGL in several points around the square (blue points in Fig. 1a) recorded PM_{10} concentrations. These measurements were taken during few minute periods (periods between 1 and 15 min) and mean values were computed for model evaluation. This is a potential issue in the comparison with model outputs representative of variables averaged over 1 h. In order to provide more information, maximum and minimum experimental values during the average period are also analyzed.

Several intercomparison tests among the instruments used were performed first at CIEMAT and later along the campaign at the measurement site, taking so into account some factors like the real particle size distribution. Grimm instrument was calibrated against gravimetric reference measurements for the three sizes PM10, PM2.5 and PM1 obtained with high volume samplers (HVS) at CIEMAT. Thus it was corrected with these factors, which include total losses in the instruments. The Grimm 1107 instrument was also compared with a TEOM at the site. Finally, to assure the homogeneity of the data, Grimm device, was also intercompared with other calibrated Grimm device prior and after the campaign. More details can be found in (Borge et al., 2016). For the analyzed summer day, PM_{10} concentrations were recorded in three different hours (from 7 to 9 LST) at eleven points around the square (Fig. 1a). At one location (point 0, Fig. 1a) PM_{10} were recorded by a Grimm instrument during these hours and at ten locations (from point 1 to 10) were measured by the portable TSI DustTrakTM. Regarding the analyzed winter day, measurements at five different hours were available (from 10 to 12 LST and from 16 to 17 LST), however depending on the hour concentrations were measured in different points (Fig. 8).

3. Multiscale system

Hourly PM_{10} concentrations are computed by means of a CFD model fed by outputs from a mesoscale meteorological model (see section 3.1) and a microscale traffic emission model (see section 3.2) (Fig. 2). These values represent 1 h-average values. Hourly PM_{10} observations from the closest urban background air quality monitoring station (located at 1.5 km away from the research area in NW direction, Fig. 1a) were used to incorporate background concentration, i.e., PM_{10} transported from any areas/ sources outside of modelling domain and, therefore not re- presented explicitly in the simulations. Inlet wind speeds and turbulent kinetic energy were taken from WRF (similar to the coupling shown in Borge et al., 2018), however in order to reduce the uncertainties of inlet wind directions in CFD simulations, hourly wind directions from the meteorological station located at a building roof (see section 2) are used as boundary conditions, i.e., a constant wind direction (mean wind direction recorded at station) was imposed at every hour in CFD si- mulations neglecting instantaneous wind direction recorded throughout each hour. This approach was used because, on one hand using both measured wind speed and direction to inflow boundary has one important disadvantage: several assumptions about the vertical wind speed profile should be done due to for the same wind speed at the height of the meteorological station, different wind speeds at other heights can be observed depending on atmospheric conditions. On the other hand, wind direction from WRF was not used because for the summer day there were notable differences between measured and modelled values (see Section 4) and CFD simulations in an urban environment are very sensitive to inlet wind direction.

This issue gives rise a new factor of uncertainty in CFD results. To use WRF wind di- rection in the CFD inlet would induce an error in the angle of the wind impacts on the building which could be important to determine the wind flow patterns within the urban canopy. Then, to minimize this effect and evaluate the other uncertainties, it was decided to impose the wind direction from meteorological station at inlet of the CFD simula- tions. Note that to apply in the inlet the WRF wind speed and measured wind direction could affect to horizontal wind shear modelled, but we consider that it is more important to have a better estimation of the wind direction to well reproduce wind flow patterns within the streets.

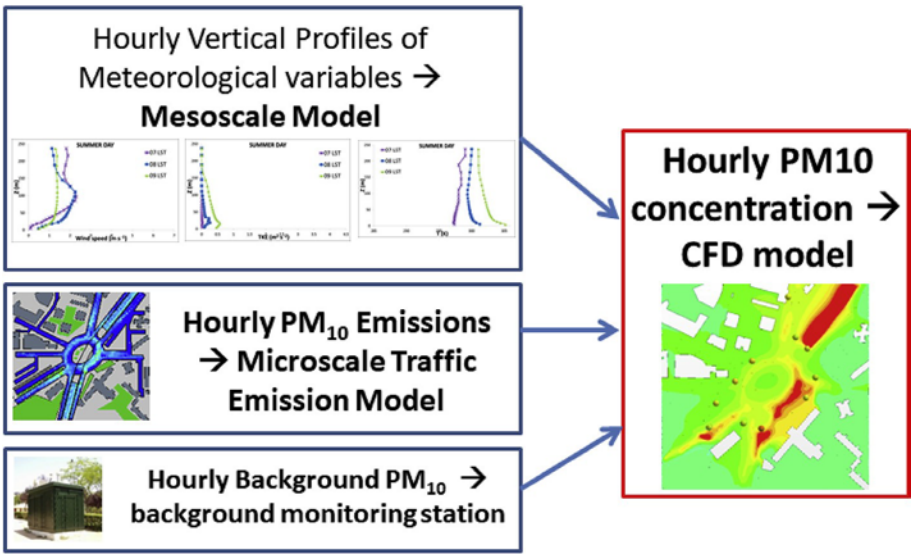

Fig. 2. Scheme of the multiscale modelling system.

For all these reasons, it is considered appropriate to use vertical profile of wind speed from WRF and measured wind direction as inflow for the CFD simulations. Modelling tools and their set-ups are explained in the next sections.

3.1. Meteorological mesoscale modelling

Mesoscale meteorological conditions of Madrid city (Spain) were simulated by means of Weather Research and Forecasting (WRF) model (Chen et al., 2011; Skamarock and Klemp, 2008) including BEP-BEM multilayer urban scheme (Martilli et al., 2002; Salamanca et al., 2010; de la Paz et al., 2016) to model the urban atmosphere. The PBL scheme of Bougeault and Lacarrere (1989) and NOAH Land Surface model (Chen and Dudhia, 2001) were used in WRF simulations. The TKE is computed taking into account the k-l closure based on Bougeault and Lacarrere (1989) coupled with the urban canopy BEP-BEM multilayer urban scheme. The definition of TKE is the same in WRF and CFD model, but in WRF it represents an average value over the grid cell of the mesoscale model (1 km × 1 km), while in the CFD this is averaged over a much smaller volume, equal to the model resolution (order of 1 m^3). Moreover, the scheme used to compute the TKE is different in the two models. In the CFD model, a k-epsilon scheme is used based on the resolution of conservation equations for TKE and its dissipation (see section 3.3). On the other hand, in WRF, the TKE is estimated by solving a prognostic equation that accounts for shear production, buoyancy production/destruction, and drag production due to the interactions between the flow and buildings. The dissipation is estimated by using a dissipation length scale, which is modified in the urban canopy. For winter simulation, four nested domains with the finest domain centered in Madrid were used with a horizontal resolution of 1 km × 1 km and 5 m of height for the lowest vertical levels (see Sanchez et al., 2017 for further details). Similar model configuration was used for summer simulation with the exception of the horizontal spatial resolution of the finest domain, which, in this case, was 500 m × 500 m. From these simulations, hourly values of vertical profiles of wind speed, temperature and turbulent kinetic energy, as well as, the sensible surface heat fluxes are outputs used by the CFD model for the two study days (25th Feb- ruary and 6th July, 2015).

3.2. Microscale traffic emission model

PM_{10} exhaust emissions are computed by means of a microscale traffic emission model (Quaassdorff et al., 2016). It is composed by: 1) PTV VISSIM model (one of the most used traffic microsimulation models in research, Fontes et al., 2015) which computed microscale traffic flows taking into account traffic restrictions like traffic lights, traffic composition and stops of public transport, 2) VERSIT+$_{micro}$ (based on ERSIT+ models for emission calculations of simulated traffic streams, Smit and McBroom, 2009) which calculated estimated high resolution exhaust emissions of individual vehicles based on speed-time profiles and vehicle types through the post-processor TNO-ENVIVER (Eijk et al., 2014) which is an interface to couple both model outputs: traffic speed-time profiles from VISSIM and microscale emissions from VERSIT+$_{micro}$. This allowed obtaining exhaust emissions aggregated to 1 h with a spatial resolution of 5 m × 5 m. Traffic emissions are com- puted in a zone of 300 m × 300 m around the square including the traffic of the road that cross the square by means of a tunnel (Fig. 1b). Real traffic camera records taken throughout the study area were used to set-up the traffic model and 12 1-h traffic emission scenarios re- presentative of different traffic conditions (traffic flow and traffic composition; see Quaassdorff et al., 2016 for further details) to re- produce traffic conditions in the research area for the two days modelled. In addition to exhaust emissions, non-exhaust emissions from pavement abrasion and brake and tire wear were estimated through the emission factors provided by the average-speed model COPERT (Ntziachristos and Samaras, 2016) according to the methodological approach discussed in Borge et al. (2018). Traffic-induced dust re- suspension was estimated following de la Paz et al. (2015). It is found that non-exhaust emissions represent 58% of total emissions, mainly from the influence of resuspension that usually dominates total emis- sions (Abu-Allaban et al., 2003). This share of non-exhaust emission is consistent with that reported by de la Paz et al. (2015) as an average for Madrid City. As vehicles become cleaner, the relative importance of combustion PM becomes smaller. According to the most updated modelling inventory (Borge et al., 2018), resuspension make up 70% of total PM_{10} emissions from road traffic. As an average, we obtained a PM10 resuspension emission factor of 82.3 mg km^{-1}, in line with the experimental estimate of Amato et al. (2010) (97 mg km^{-1}) for Barce- lona urban area. Previous studies have estimated resuspension factors across Europe from 17 mg km^{-1} to 222 mg km^{-1} (Gehrig et al., 2004; Ketzel et al., 2007; Bukowiecki et al., 2010) while Abu-Allaban et al. (2003) reported resuspension emission factors from 40 to 780 mg km^{-1} for light vehicles and 230–7800 mg km^{-1} for heavy-duty vehicles in the US. Road salt and studded tires used in northern countries may produce considerably higher resuspension factors (Ferm and Sjöberg, 2015). Finally, all non-exhaust emissions were consistently disaggregated to a

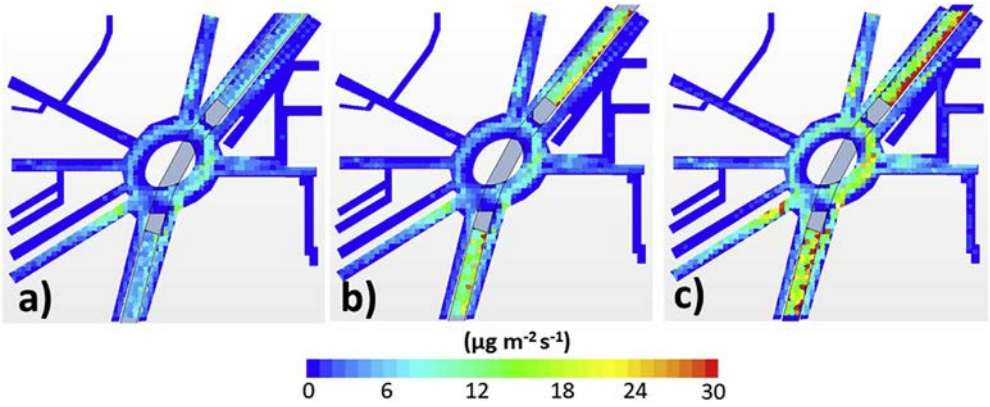

Fig. 3. PM_{10} emissions for 7 LST in summer. a) Exhaust emissions, b) non-exhaust emissions and c) total emissions.

spatial resolution of 5 m × 5 m considering real traffic conditions and added to PM_{10} emissions from the pipe tails. The spatial disaggregation of the emissions into the 5 m × 5 m modelling mesh in the example illustrated in Fig. 3 yields an average emission factor (please note that emissions are exclusively assigned to paved surfaces) of 5.3 µg m-2 s-1 in the roundabout and 24.8 µg m-2 s-1 in the tunnel (2.2 and 17.9 µg m-2 s-1 for non-exhaust emissions respectively). Emissions reach values close to 30 µg m-2 s-1 but only in some specific grid cells, as illustrated in Fig. 3. Then, within the uncertainty of traffic emission factors we are confident that emission inputs are realistic. All traffic-related PM_{10} emissions were allocated in CFD simulation from ground to 1 m AGL. Maps illustrating resulting PM_{10} emissions of 1-h scenario (exhaust, non-exhaust and total emissions) are shown in Fig. 3. In the CFD model domain, only traffic emissions are considered. Domestic heating emis- sions in the study zone are neglected because they emitted at con- siderable height and are not so relevant for ground-level concentrations within such a small domain. On the other hand, emission sources lo- cated outside the domain like domestic heating outside the study zone or Saharan dust intrusions are taken into account by means of hourly background concentration recorded at urban background monitoring station.

3.3. *CFD model*

The CFD model used (STAR-CCM+, Siemens) is based on Reynolds-Averaged Navier-Stokes (RANS) equations with Realizable *k*-ε turbu- lence scheme, where *k* and ε are the turbulent kinetic energy and its dissipation rate. This turbulence scheme is based on the resolution of conservation equations for turbulent kinetic energy and its dissipation. Shear and buoyancy sink/source terms are considered in the turbulent kinetic energy equation, as well as the mean and turbulent transport. Although Large Eddy Simulations (LES) are more accurate, they also require much higher computational resources (Santiago et al., 2010; Dejoan et al., 2010; Blocken, 2018). In this study, RANS is selected as a compromise between accuracy and computational requirements. A sink term was added to the momentum equations in order to model aero- dynamic effects of vegetation (green zone in Fig. 1b) on wind flow. Also sink/source terms were included in the turbulent kinetic energy and ε equations in the computational cells including vegetation (Santiago et al. 2017b, 2017c, 2019; Buccolieri et al., 2018). Non-isothermal si- mulations were performed with an equation for temperature (energy conservation equation) solved and Boussinesq's approach used for ac- counting buoyancy effects. This approximation considers the air density constant except for the buoyancy term where changes in the density (ρ), are expressed in terms of temperature (*T*), thermal expansion coeffi- cient (β) and the gravitational vector (g) as $\rho \boldsymbol{g} \beta \Delta T$. PM_{10} dispersion is modelled by means of a transport equation (Equation (3)).

$$\frac{\partial C}{\partial t} + u_j \frac{\partial C}{\partial x_j} = D \frac{\partial^2 C}{\partial x_j \partial x_j} + \frac{\partial}{\partial x_j}\left(K_c \frac{\partial C}{\partial x_j}\right) + S_C \quad (3)$$

where *C* is PM_{10} concentration, *D* is the molecular viscosity, S_C is the source term to represent emissions and K_c is the eddy diffusivity of pollutant that is $K_c = \mu_t / S_{ct}$, being S_{ct} the turbulent Schmidt number and μ_t the turbulent eddy viscosity. The turbulent Schmidt number used has an impact on the pollutant dispersion simulations and the modelled concentrations depend on the selected value (Di Sabatino et al., 2007; Tominaga and Stathopoulos, 2007; Gromke et al., 2008; Vranckx et al., 2015; Gromke and Blocken, 2015; Rivas et al., 2019). Tominaga and Stathopoulos (2007) pointed out that its optimum value is between 0.2 and 1.3 depending on flow properties and geometries and, for a simple geometry, Vranckx et al. (2015) found a different optimum S_{ct} (from 0.3 to 1) depending on wind direction. Sanchez et al. (2017) using $S_{ct} = 0.3$ found a good CFD model performance simulating NO_X dispersion over the same urban domain as this study, however no sensible surface heat fluxes were considered in that study. In this work, the dependence of S_{ct} on computed concentrations is analyzed comparing results from simu- lations using two different values (0.3 and 0.7). The decrease or in- crease of turbulent Schmidt number allows increasing or decreasing the diffusivity, respectively.

The study zone is modelled taking into account the real building geometry and layout, vegetation areas and emission zone (Fig. 1b). The numerical domain size was 1300 m × 1300 m x 270 m, which was built considering the best practice guideline of COST Action 732 (Di Sabatino et al., 2011). This domain was discretized by means of an irregular grid of 8.3×10^6 computational cells. The average resolution was around 2 m in each direction with mesh refinements close to the ground buildings and the emission zones, cells smaller than 1 m^3 were used (Fig. 1c). The grid size progressively increases to 5 m outside from the study area with an expansion ration lower than 1.3. A mesh in- dependence test was performed concluding that this grid is appropriate to solve wind flow in this area (Sanchez et al., 2017).

CFD simulations from 6 Local Solar Time (LST) to 18 LST of 25th February and 6th July were carried out. Buildings and ground were considered as wall boundary conditions and symmetry conditions were imposed at the top of the domain. Inlet and outlet boundaries were defined depending on inlet wind direction. Inlet conditions were kept constant during each hour. Hourly vertical profiles of meteorological variables model were imposed from the mesoscale model except the wind direction. In particular, hourly vertical profiles of wind speed, temperature (*T*) and turbulent kinetic energy (*k*) are taken from the mesoscale cells corresponding to microscale domain. Fig. 4 shows the vertical profiles corresponding to the hours of winter and summer days when PM_{10} dispersion is simulated. Concerning ε, since it is not directly computed by WRF, their values were calculated from its relation with turbulent kinetic energy as $\varepsilon = C_\mu \, k^{3/4} / (\kappa z)$, where *z* is the height, $C_\mu = 0.09$ and $\kappa = 0.4$. The effect of sensible surface heat fluxes (SHF),

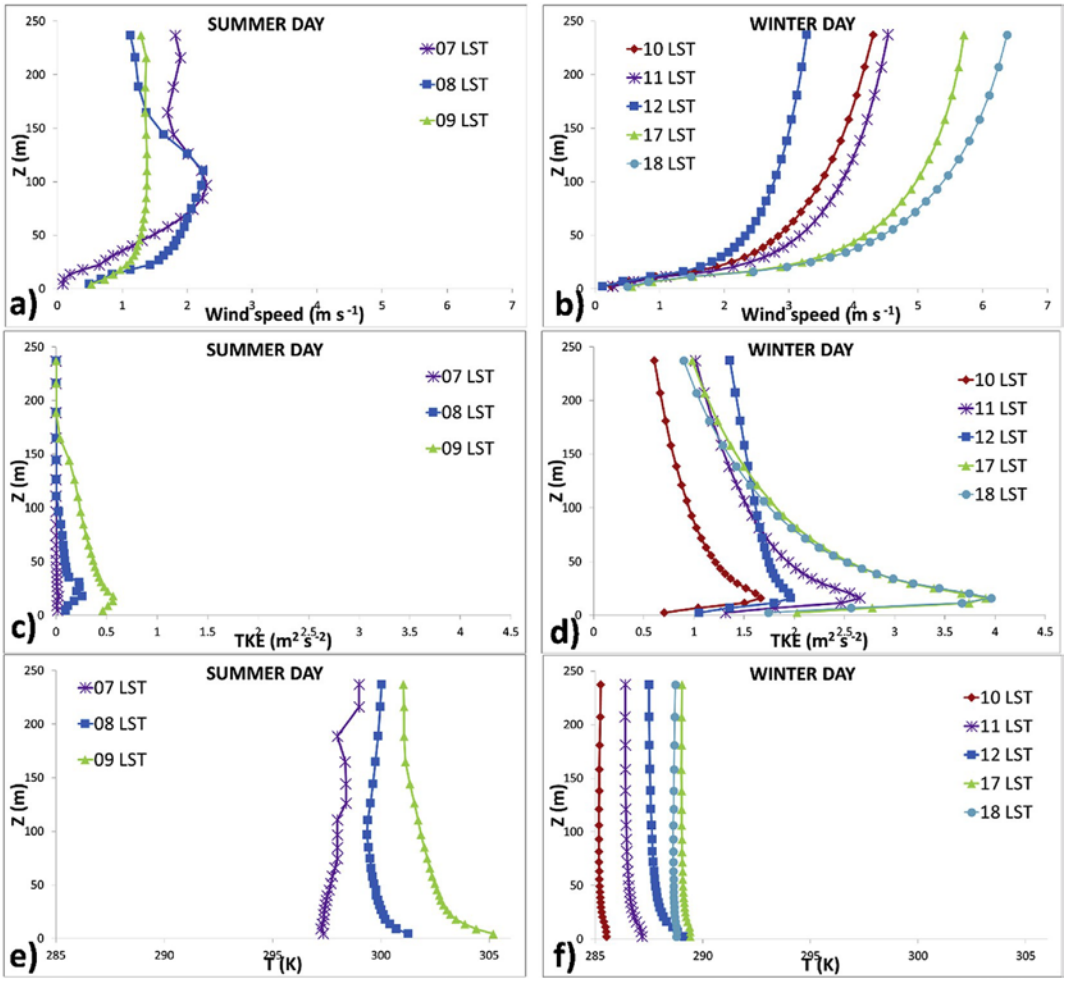

Fig. 4. Inlet profiles imposed at CFD simulations. a) wind speed for summer day; b) wind speed for winter day; c) TKE for summer day; d) TKE for winter day; e) T for summer day; f) T for winter day.

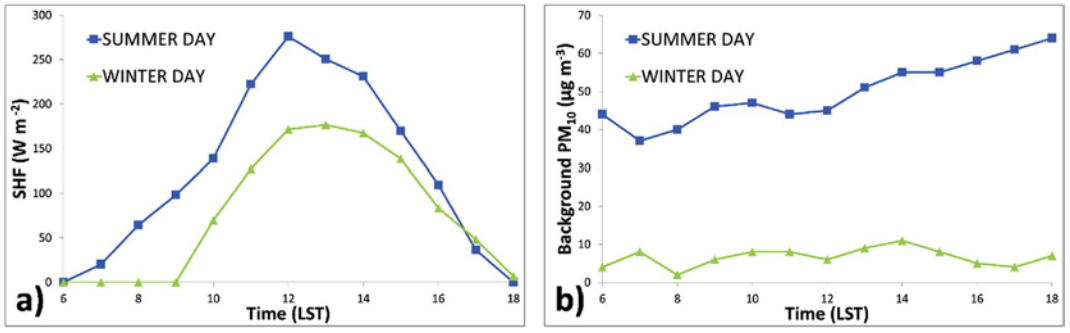

Fig. 5. a) SHF computed by WRF and imposed at ground in CFD simulations during both studied days. b) Background PM10 concentration measured at the closest urban background air quality monitoring station during both studied days.

usually not considered in CFD simulations, was also studied in this paper. As commented in the introduction, some CFD studies, without coupling with mesoscale models, applied SHF into building walls and/ or ground (Qu et al., 2012; Yaghoobian and Kleissl, 2012; Santiago et al., 2014; Nazarian et al., 2018). In this paper, to account for this in a simple way avoiding the extra computational burden of a solar radiation model, hourly SHF computed by WRF is imposed at the ground level in the CFD simulation. Then, the ground boundary in each CFD simulations releases a sensible surface heat flux equals to the corresponding SHF computed by WRF at this hour, which is uniformly distributed in the CFD simulations. Fig. 5a shows hourly SHF computed by WRF and imposed to the ground of each hourly CFD simulations for the summer and winter day. As expected, it is observed greater SHFs and earlier sunrise for the summer day. Simulations without considering SHF (assuming surfaces as adiabatic) were also performed in order to evaluate the impact of neglecting SHF on the results. The wind direction is assumed constant vertically and changed every hour taking the value from the reference meteorological station (red point in Fig. 1a). There is a shift between measured values and mesoscale wind directions at some hours, and this assumption minimizes the inlet wind direction uncertainties and their influence on the CFD results.

Concerning the boundary conditions for PM_{10}, hourly background

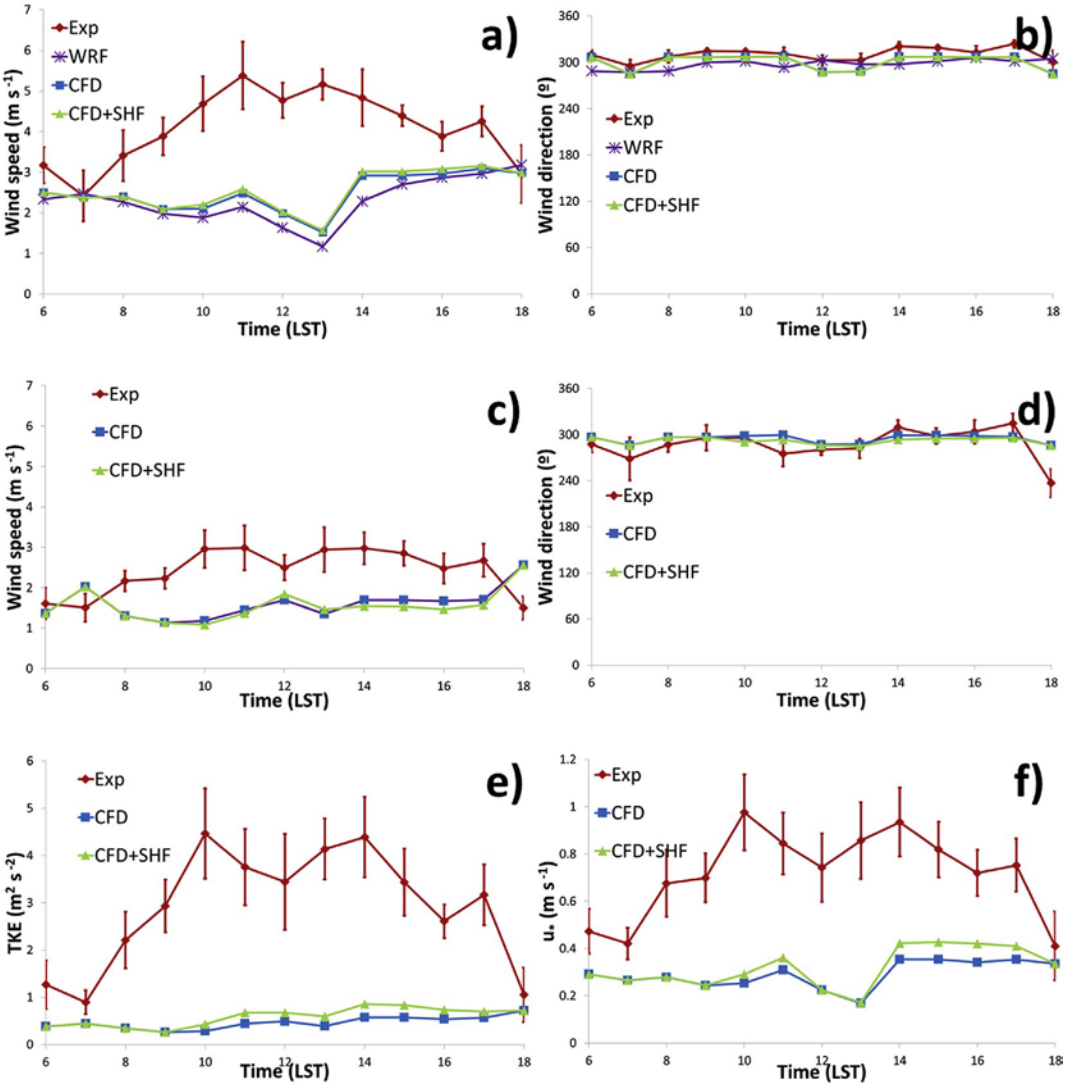

Fig. 6. Experimental data and modelled results for 25th February. a) wind speed and b) wind direction on the building roof location; c) wind speed, d) wind direction, e) turbulent kinetic energy and f) friction velocity at the location of sonic anemometer 1 (orange point of Fig. 1 at 8 m AGL). Vertical bars indicate standard deviation of experimental mean values within each hour.

concentrations were taken from the closest urban background air quality monitoring station (Fig. 1a) which is located at 1.5 km away from the research area in NW direction (Fig. 5b). This is the same approach was used by Sanchez et al. (2017) to model NO_X in this area with satisfactory results. The emission zone in CFD simulations is located in the roads from the ground up to 1 m-height within an area of 300 m × 300 m around the square (Sanchez et al., 2017). Here, the total emissions of PM_{10} (exhaust and non-exhaust emissions) at each hour are imposed. The emissions computed by traffic emission model in a regular grid of 5 m × 5 m are distributed in the CFD mesh (with higher resolution) using a mass-conservative interpolation scheme (Fig. 3). The emissions were updated every hour in CFD simulations implementing the emission scenario corresponding to each hour following the local-specific pattern defined by Quaassdorff et al. (2016) and Sanchez et al. (2017). Of note, both study days were working days.

4. Results and discussion

Firstly, the comparison of measured and modelled wind speed and directions at the location of reference meteorological station, which are representative of meteorological conditions above the street level, was performed to evaluate the inlet meteorological conditions of CFD simulations (section 4.1). Similarly, in this section, modelled meteorological parameters (wind speed and direction, turbulence kinetic energy and friction velocity) at the street level were evaluated through a comparison with sonic anemometer measurements. Here we also dis- cuss the impact of the CFD inlet wind profiles uncertainties on the microscale model performance depending on the approach used (ne- glecting or accounting for sensible surface heat fluxes). Finally, in section 4.2, PM_{10} dispersion is simulated by our CFD model using different approaches (neglecting or accounting for surface heat fluxes and changing turbulent Schmidt number). Modelled PM_{10} concentrations are evaluated against observations recorded at different locations and hours in order to discuss the performance of each approach.

4.1. Evaluation of CFD simulation results: meteorological parameters at street level

Mesoscale meteorological conditions were included in CFD simulations through inlet meteorological conditions, and then CFD model performance depends on the accuracy of these imposed inlet conditions. Information about mesoscale meteorological conditions were available from the meteorological station located on the building roof (Fig. 1a) and from WRF simulations. This meteorological station recorded wind

speeds and directions which are representative of meteorological con- ditions above the street levels, except for some wind directions where wind can be partially sheltered by taller buildings located in the South of the station. On the other hand, WRF simulations provide vertical profiles of flow properties (wind speed and direction, temperature and turbulent kinetic energy) which are representative of the horizontal spatial averages over the mesoscale grid cells. In CFD simulations, hourly wind directions were assumed constant vertically. Due to the differences at some hours on the 6th July found between measured and WRF values on the building roof (Fig. 7b), and with the aim of minimizing the uncertainties of CFD simulations due to the inlet conditions, wind directions were taken from the reference meteorological station instead of from WRF simulations. Additionally, the vertical variations of speed, temperature and turbulence were considered taking the vertical profiles from WRF as CFD inlet conditions. As explained in section 3, we consider the best option to use vertical profile of wind speed from WRF and measured wind direction as inflow for CFD simulations.

Firstly, the evaluation of inlet meteorological conditions imposed at CFD were performed comparing hourly mean wind speeds and directions recorded on the meteorological tower located on building roof against CFD results at this location (6a-6b and 7a-7b). Wind speeds and directions obtained from the WRF simulations on the building roof were also compared to check the differences between wind speeds above the street level imposed at the CFD at inlet and actual wind speeds. In addition, hourly standard deviations of measurements are also plotted in Figs. 6 and 7 as vertical bars to obtain information about fluctuations of wind speed and direction during each hour. It is noteworthy that WRF results represents the horizontally spatial averaged flow properties over the mesoscale cell, in this comparison at 18 m AGL. However, CFD spatial resolution is much higher and in this case the values of wind speed and directions are extracted from the CFD simulations in the computational cell corresponding to the location of meteorological station. Then, the objective of this comparison is to check that the wind direction is not perturbed by any obstacle from the inlet to the meteorological tower and it is suitable to be used as inlet wind direction. Results from CFD with and without taking into account surface heat fluxes are also shown in Fig. 6a, b, 7a and 7b. In addition, to quantify the model agreement with measurements data, some statistic metrics (normalized mean square error, NMSE; factor 2, FAC2 and fractional BIAS, FB) were computed (Table 1).

$$NMSE = \frac{\sum_1^n (P_i - O_i)}{\sum_1^n P_i \sum_1^n O_i} \quad (4)$$

$$FB = \frac{\sum_1^n P_i - \sum_1^n O_i}{0.5(\sum_1^n P_i + \sum_1^n O_i)} \quad (5)$$

where n is the number of measurements, P_i are the modelled values and O_i are the measurements. NMSE provides information about the mean

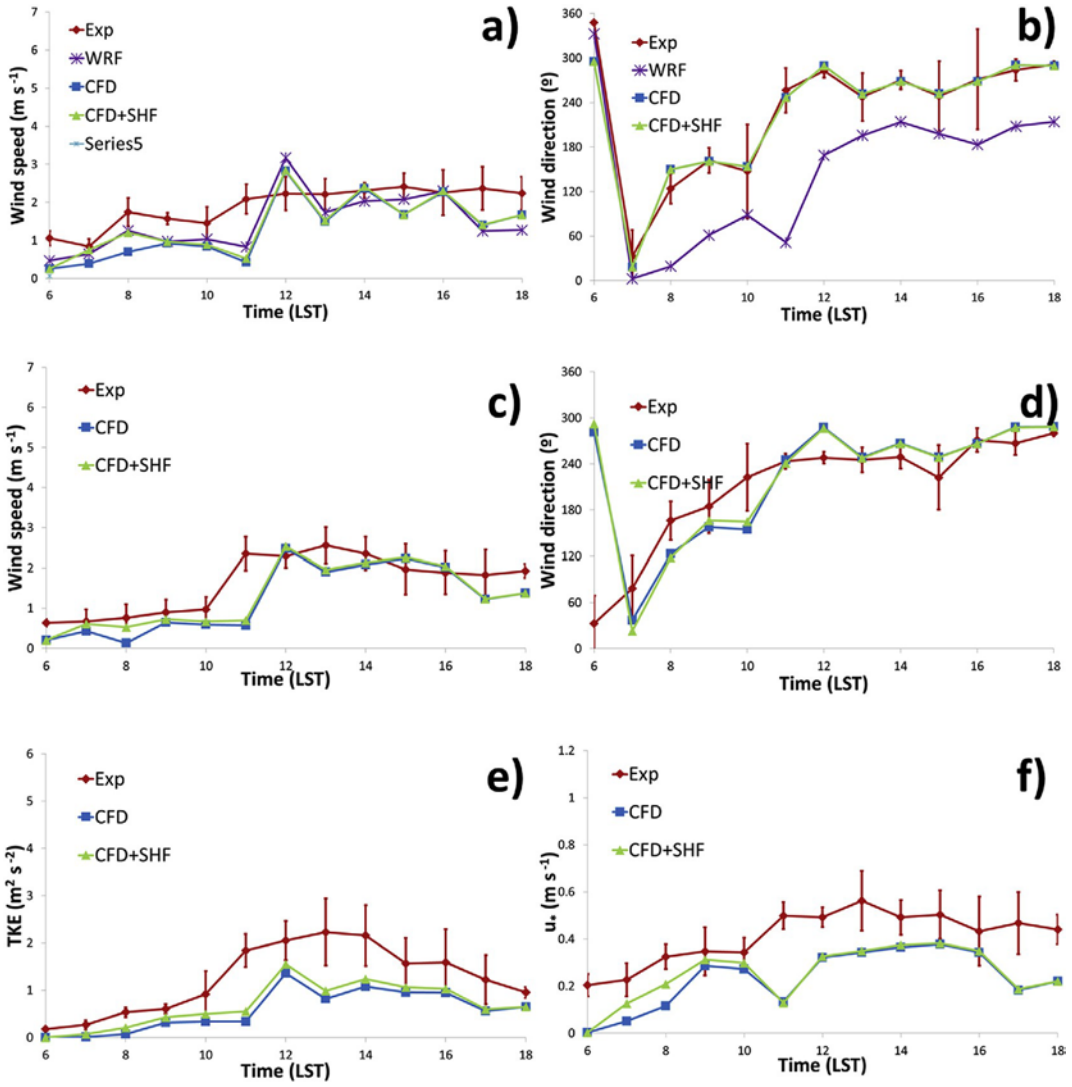

Fig. 7. Same as Fig. 3 but for 6th July.

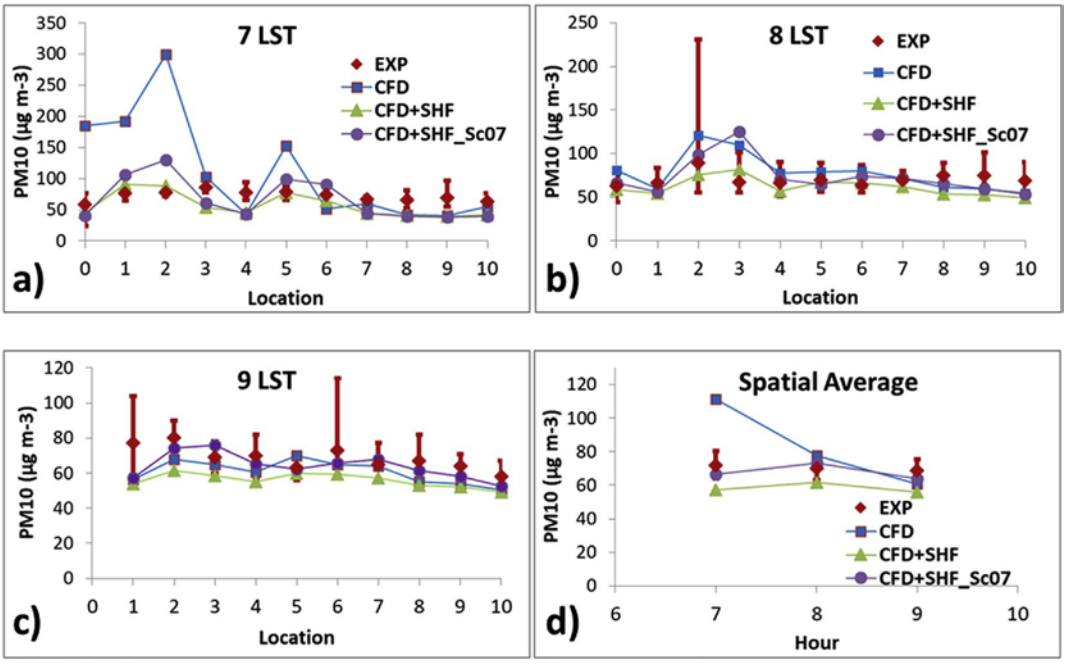

Fig. 8. a) Modelled and measured PM_{10} concentration at 7 LST of 6th July 2015. b) and c) the same as a) but for 8 LST and 9 LST respectively. Vertical bars represent the range of experimental PM_{10} concentration fluctuations at each position. d) Average concentration over all locations.

Table 1
Statistic metrics computed from the different modelling approaches results for meteorological measurements above the street levels (the reference meteorological station on the building roof). Note that wind speed is always positive because it is the magnitude of wind velocity computed from velocity components obtained.

	WINTER			SUMMER			TOTAL		
	NMSE	FB	FAC2	NMSE	FB	FAC2	NMSE	FB	FAC2
Wind Speed (CFD)	0.37	−0.49	0.69	0.25	−0.36	0.69	0.38	−0.44	0.69
Wind Speed (CFD+SHF)	0.34	−0.47	0.69	0.19	−0.29	0.84	0.34	−0.41	0.77
Wind Direction (CFD)	0.001	−0.03	–	0.006	−0.01	–	0.003	−0.02	–
Wind Direction (CFD+SHF)	0.001	−0.03	–	0.006	−0.01	–	0.003	−0.02	–

Table 2
Statistic metrics computed from the different modelling approaches results for meteorological measurements at the street levels (sonic anemometer locations).

	WINTER			SUMMER			TOTAL		
	NMSE	FB	FAC2	NMSE	FB	FAC2	NMSE	FB	FAC2
Wind Speed (CFD)	0.31	−0.37	0.85	0.19	−0.22	0.77	0.28	−0.30	0.81
Wind Speed (CFD+SHF)	0.35	−0.39	0.80	0.15	−0.15	0.85	0.28	−0.29	0.83
Wind Direction (CFD)	0.004	−0.01	–	0.07	0.00	–	0.03	−0.01	–
Wind Direction (CFD+SHF)	0.004	−0.02	–	0.08	0.00	–	0.03	−0.01	–
TKE (CFD)	5.52	−1.45	0.12	0.92	−0.75	0.42	3.72	−1.20	0.27
TKE (CFD+SHF)	3.91	−1.33	0.12	0.57	−0.60	0.54	2.68	−1.06	0.33
u_*(CFD)	1.15	−0.89	0.19	0.44	−0.59	0.58	0.93	−0.77	0.38
u_*(CFD+SHF)	0.93	−0.81	0.31	0.36	−0.51	0.73	0.76	−0.69	0.52

error and FB about underestimation (negative values) or overestimation (positive values). For dispersion model results, Chang and Hanna (2004) recommended NMSE < 4, FAC2 > 0.5 and $-0.3 <$ FB < 0.3 for considering a good agreement. However, this criteria was modified by Hanna and Chang (2012) for urban applications proposing NMSE < 6, FAC2 > 0.3 and $-0.67 <$ FB < 0.67.

For both days, wind directions and wind speeds obtained from CFD simulations at this location are similar to the inlet values imposed at this height, i.e. wind directions similar to the measurements recorded from the station and wind speeds similar to WRF values at this height. Then, wind directions and speeds at this height imposed at inlet boundaries are barely disturbed by urban morphology from the boundaries to the station location. Therefore, using measured wind direction from meteorological station as inlet wind direction is considered appropriate. On 25th February, modelled wind speed is underestimated indicating an underestimation of inlet wind speed in the CFD simulations. For the 6th July simulation, the agreement between observations and CFD results was improved, despite a slight underprediction of the model (NMSE and FB decrease for both CFD approaches). The standard deviation of experimental mean values show that fluctuations of wind speed and direction during each hour could be considerable increasing the uncertainties of CFD inlet conditions where these effects are neglected.

Once inlet conditions have been checked that are appropriate,

meteorological parameters at street levels obtained by CFD are eval- uated. Modelled mean wind speed and direction and two important turbulence variables, turbulent kinetic energy (*TKE*) (Equation (1)) and friction velocity (u_*) (Equation (2)) were evaluated at the street level by means of a comparison against hourly average measurements recorded from the sonic anemometers (Fig. 1a) for both study days (Figs. 4 and 5 and Table 2). Note that at the street levels the horizontal spatial heterogeneities of meteorological parameters are strong, and here, the comparison could be only performed in one location at two similar height (6 and 8 m AGL). However, CFD results were extracted from the cells where the sonic anemometers were located with an accuracy of about 1 m, and then the evaluation were performed at the same positions. Since a *k*-ε turbulence scheme was employed, modelled turbulent kinetic energy was directly extracted from CFD model. However, to compute the friction velocity, turbulent momentum fluxes ($u'w'$ and $v'w'$) were calculated by relating Reynolds stresses to the mean velocity gradients, namely:

$$-\overline{u_i'u_j'} = \frac{1}{\rho}\mu_t\left(\frac{\partial u_i}{\partial x_j} + \frac{\partial u_j}{\partial x_i}\right) - \frac{2}{3}TKE\delta_{ij} \quad (6)$$

where μ_t is the dynamic viscosity expressed as $\mu_t = \rho C_\mu \frac{TKE^2}{\varepsilon}$.

Similar experimental values were observed with both anemometers, with slightly lower values of wind speed, TKE and friction velocity at sonic anemometer 2 (6 m AGL). Additionally, similar performances of CFD simulations were found. In Fig. 4c–f and 5c–f only results from sonic anemometer 1, located at 8 m AGL, are shown, but the statistical metrics (Table 2) were computed using data from both sonic anemometers. Both days, hourly mean wind direction is well reproduced at the street level. Regarding mean wind speed at the street level, it is better reproduced by the CFD model for the 6th July than for the 25th February, where an underestimation is observed. This issue seems to be related to inlet wind conditions imposed in CFD simulations. For the 25th February, wind speed imposed above the street level is lower than the actual wind speed (Fig. 4a) and as a consequence the CFD values computed at the street level (sonic anemometers) (Fig. 5c) are under- estimated in the same range than above the street level (Tables 1 and 2). However, for the 6th July, better inlet wind speed conditions are imposed and then wind speed is better reproduced. In general, similar model performances (Tables 1 and 2) are found on the building roof location and at the street level (sonic anemometers). Comparing CFD simulations with different approaches, slightly better fit with experimental results is obtained when surface heat flux from WRF is imposed at ground in CFD (Table 2).

Turbulent parameters (*TKE* and u_*) are underpredicted, particularly for the winter day (25th February) simulation. This behavior can be related to underestimation of mean wind speed, but also to the *k*-ε approach of CFD model, including uncertainties of inlet turbulence conditions and/or processes which are not well represented in the model such as turbulence induced by vehicles or heat fluxes (Solazzo et al., 2008; Alonso-Estébanez et al., 2012). Unfortunately, turbulent parameters above the street level was not measured and inlet turbulence conditions could not be evaluated. Comparing measurements for winter and summer, TKE at street level in winter is almost double than TKE in summer, while wind speed is similar at the street level for both days. On the other hand, the wind speed measured on the building roof (18 m AGL) is double in winter than in summer. Likely it is the vertical gradient of wind speed that produces more TKE in winter than in summer. Therefore, this turbulence production could not be captured by CFD simulations due to an underestimation of wind speed vertical gradient of the inlet vertical profile imposed. For the 6th July simulation, where the mean wind speed is well predicted, the turbulent parameters are in better agreement with the experimental values, obtaining a better fit when surface heat fluxes from WRF are imposed at ground (reduction of FB for TKE and u_*, Table 2). This fact is important for pollutant dispersion, particularly at certain hours where the turbulent kinetic energy obtained without considering SHF is almost 0 and mean wind speed is low (e.g. 8 LST for 6th July). Here, the con- centration would be overestimated if SHF is not considered in the simulation. In this summer day, a slight underestimation of turbulent parameters is observed which could be due to the reasons discussed above. Overall, CFD simulations reproduced the wind flow properties recorded by sonic anemometers, in particular on the summer day and taking into account SHF at ground.

4.2. Evaluation of CFD simulation results: particulate matter concentrations at street level

Wind flow patterns determines pollutant distribution within urban canopy, and then the evaluation of modelled micrometeorology, de- scribed in the previous section, is important for assessing the model performance of pollutant dispersion. The dispersion of PM10 is modelled by means of the transport equation. The difference of PM10 dispersion between wintertime and summertime cases are due to there are different meteorological conditions, including the background concentrations, between both days. Wind speed and direction have influence on the mean transport of pollutant and TKE in the turbulent transport taking into account that the eddy diffusivity is related to the turbulent eddy viscosity ($K_c = \mu_t/S_{ct}$), and then with TKE ($\mu_t = \rho C_\mu \frac{TKE^2}{\varepsilon}$). In addition, temperature profile induces a buoyancy force in vertical direction changing the mean transport of pollutant, and produces TKE, which have influence on turbulent transport of the pollutant. In addition to simulations neglecting or accounting for sen- sible surface heat fluxes (SHF), PM10 dispersion is simulated for two different turbulent Schmidt values (0.3 and 0.7). PM_{10} concentrations modelled with different approaches at the 3 h of the summer day where measurements are available (see section 2) are shown in Fig. 8. Additionally, as in the previous sections, to evaluate the agreement be- tween modelled and measured PM_{10} concentrations, statistic metrics (NMSE, FB, FAC2) are computed for the different modelling approaches (Table 3). For the studied summer day, concentration differences be- tween approaches are higher at 7 and 8 LST, obtaining a better performance for CFD simulations including SHF and $S_{ct} = 0.3$. Although SHF at these hours and its influence on wind speed and turbulence kinetic energy are not high, SHF provides a notable impact on PM_{10} dispersion because in the case where it is neglected the wind speed and turbulence are extremely low. In this day, to take into account the surface heat fluxes in simulations seems to be more important than the value of S_{ct}, at least in this range. Although a low S_{ct} is used (0.3), the concentration overestimation in CFD simulations without accounting for SHF is greater than in simulations including SHF with a higher S_{ct}

Table 3
Statistic metrics computed from the PM_{10} concentrations obtained with the different modelling approaches.

PM_{10}	WINTER			SUMMER			TOTAL		
	NMSE	FB	FAC2	NMSE	FB	FAC2	NMSE	FB	FAC2
CFD (NO SHF; $\mathbf{S_{ct}}$ = 0.3)	0.53	0.27	0.83	0.49	0.17	0.91	0.59	0.19	0.88
CFD (SHF; $\mathbf{S_{ct}}$ = 0.7)	0.98	0.46	0.56	0.09	−0.03	1.0	0.17	0.05	0.84
CFD (SHF; $\mathbf{S_{ct}}$ = 0.3)	0.25	0.08	0.83	0.07	−0.19	1.0	0.09	−0.15	0.94

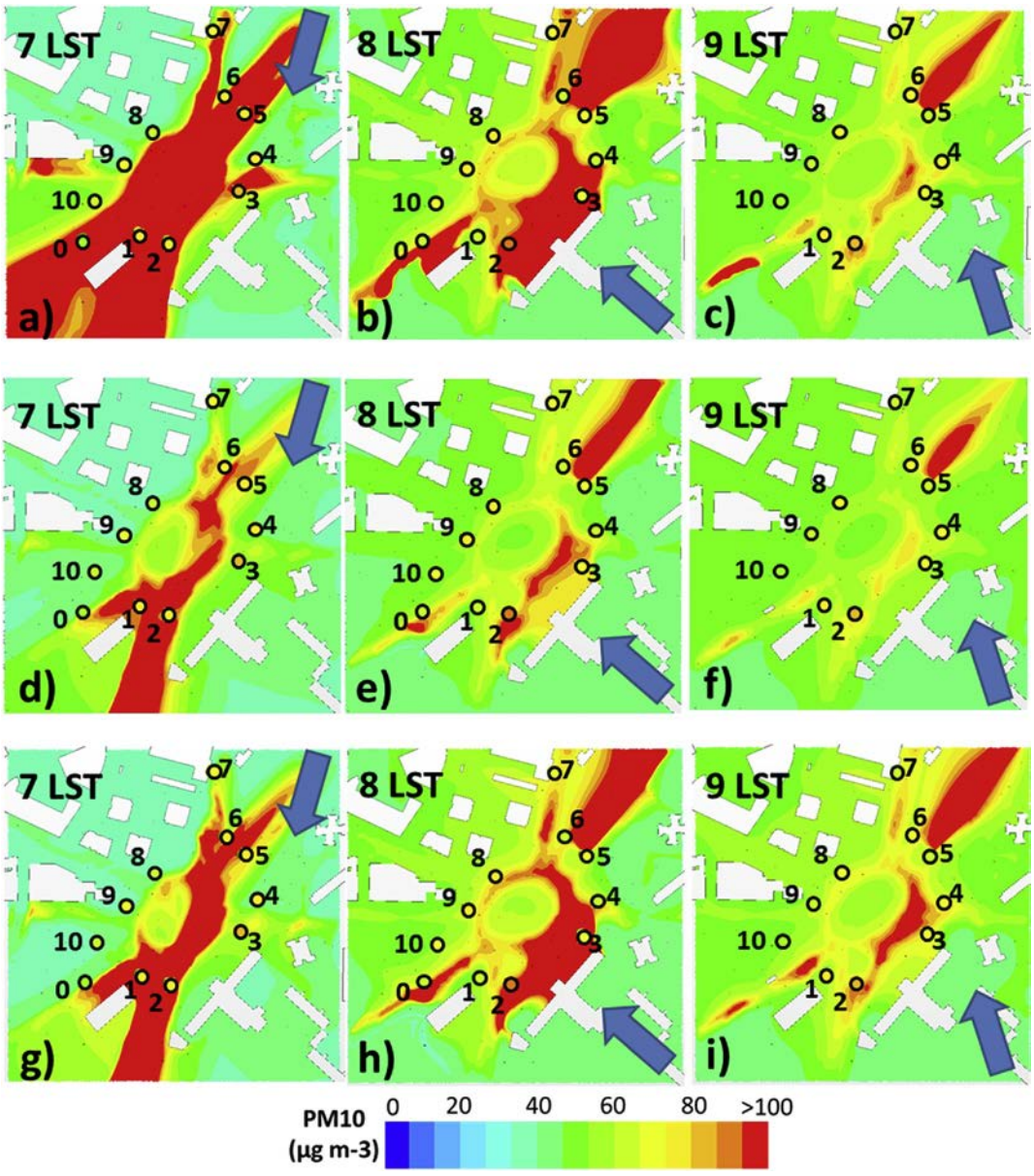

Fig. 9. Modelled PM_{10} concentration at pedestrian level (1.5 m AGL) for 6th July 2015. a) Simulation neglecting SHF and S_{ct} = 0.3 for 7 LST, b) same as a) but for 8 LST, c) same as a) but for 9 LST. d) Simulation accounting for SHF and S_{ct} = 0.3 for 7 LST, e) same as d) but for 8 LST, f) same as d) but for 9 LST. g) Simulation accounting for SHF and S_{ct} = 0.7 for 7 LST, h) same as g) but for 8 LST, i) same as g) but for 9 LST. The colour of points indicates the measured concentration at each location and the blue arrows represent the inlet wind direction.

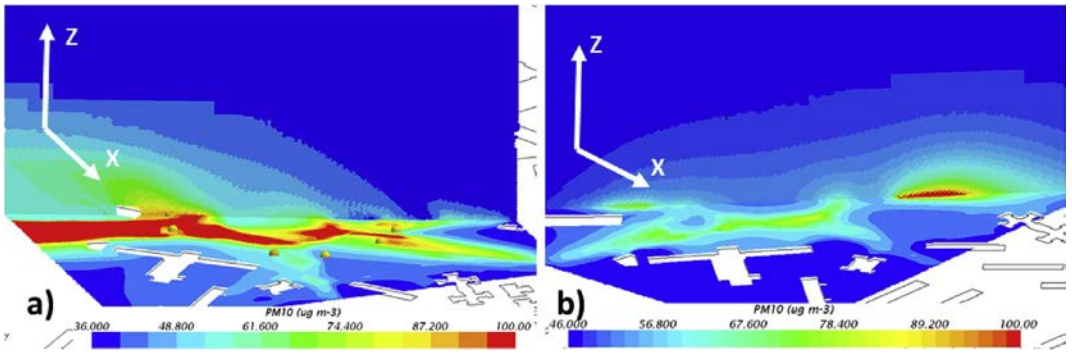

Fig. 10. Modelled PM_{10} concentration at horizontal plane at pedestrian level (1.5 m AGL) and at vertical plane for 6th July 2015. a) Simulation with SHF and S_{ct} = 0.3 for 7 LST, b) same as a) but for 9 LST.

(= 0.7), in particular at 7 LST. Table 3 shows as FB is greater for simulations neglecting SHF and the average concentration in all points at each hour (Fig. 8d) also shows the concentration overestimation of this approach. Fig. 9 show modelled PM_{10} concentration maps at pedestrian level for the three approaches (NO SHF, SHF and S_{ct} = 0.3 and SHF and S_{ct} = 0.7) and the experimental value (coloured points). The pedestrian level is considered 1.5 m AGL, which is the height where measurements were recorded with the portable TSI DustTrakTM. Strong modelled
concentration gradients are observed for all simulations, particularly higher for simulations neglecting SHF. This is usually found close to roads (Borge et al., 2016; Santiago et al., 2017a,b,c). These strong gradients could be overestimated in simulations due to the impact of not modelling the inlet wind flow fluctuations (Fig. 5a) during the hour. Simulations are carried out accounting for a constant inlet wind di- rection during each hour, but the fluctuations of wind direction can be significant during 1 h, in particular this is observed in the analyzed summer day. Additionally, concentration fluctuation are also found (Fig. 6). Their relative magnitudes are high, even in some cases can achieve 100% of the average value. These fluctuations are related to not only wind direction fluctuation but also quick changes in traffic emis- sions. This issue indicates that non-stationary simulations with changes of inlet conditions (wind flow and emissions) in periods shorter than 1 h could improve simulation results in future studies. To illustrate the vertical distribution of PM_{10} and its relationship with atmospheric conditions PM_{10} concentration at a vertical plane for 7 LST and 9LST of the summer day is shown in Fig. 10. At the inlet conditions for 7 LST and 9 LST (Fig. 4), it is observed that wind speed at the height of the meteorological tower is lower than 1 m s^{-1} in both cases being the wind speed and the TKE at lower heights higher at 9 LST. In addition, the vertical profile of temperature close to the ground is unstable at 9 LST, while it is slightly stable at 7 LST. Another important factor is that SHF imposed at ground is much higher at 9 LST than at 7 LST. All these factors lead to a reduced PM_{10} dispersion at 7 LST compared to 9 LST. This can be observed in Fig. 10 where the concentration is higher at all heights even if the same pollutant emissions were imposed at ground (emissions at both hours are the same). In the case of the winter day, a suitable model performance for PM_{10} concentration is only obtained for
simulations including SHF and S_{ct} = 0.3, although with a slight over-estimation in some points due to wind speed and turbulence under-estimation (Table 3 and Figs. 11 and 12). However, although some flow variables were not well reproduced, concentrations were more or less better reproduced. This is according to some results obtained in COST Action 732 exercises (Schatzmann et al., 2010).

5. Summary and conclusions

A multi scale modelling system including high resolution traffic emissions is applied to a real traffic hot-spot in Madrid (Spain). Modelled micrometeorology and PM_{10} concentrations are evaluated using measurements from experimental campaigns (one in winter and one in summer) carried out in the study zone. The modelling system is able to reproduce pollutant concentration recorded during the two days analyzed, however model performance is better for summer day due to the better inlet conditions imposed to CFD simulations. More specific findings are as follows:

1) Mesoscale inlet meteorology in CFD simulations. Prior to comparing concentrations, modelled meteorological variables should be evaluated (if experimental data are available) in order to analyze whether the differences with measured concentrations are related to the wind flow or the dispersion representation. Additionally, part of these differences may be induced by uncertainties in the inlet conditions. In this paper, it is observed that the model performance is improved when appropriate mesoscale wind flow conditions are implemented in the CFD simulations (summer day). However, in general, CFD simulations underestimate turbulence variables.
2) Surface heat fluxes. This effect is often neglected in CFD simulations. A detailed computation of heat fluxes emitted by urban surfaces at microscale needs the implementation of a realistic radiation model which would increase the required computational time. However, in this paper it is found that a simple approach imposing SHF provided by a mesoscale model at ground level in the CFD simulations im- proves the model performance. This is particularly important in low wind and low turbulence conditions as in the early morning hours simulated in the analyzed summer day.
3) Turbulent Schmidt number. The impact of this coefficient, which relates to the turbulent eddy viscosity and pollutant eddy diffusivity, on concentrations is analyzed taking into account that measure- ments of meteorological variables are reproduced by CFD when appropriate inlet boundary conditions are used. As the turbulent kinetic energy is underestimated, possibly due to uncertainties of inlet turbulence mesoscale conditions and/or some processes which are neglected in the simulations (e.g. turbulence induced by traffic, heat emitted by vehicles, etc.), simulations with low value of S_{ct} (=0.3) performed better, in particular under low wind and low turbulence conditions.
4) Temporal variability of inlet conditions. Wind and PM_{10} concentrations presents significant variability within 1-h periods. This may be due to changes of the mesoscale meteorology and the traffic conditions and therefore, emissions. This is one of the main limita- tion of this study. That would suggest that shorter modelling periods (e.g. 15–30 min) or a non-stationary approach may further improve the modelling results, and thus, this one of future research line. This approach requires, in addition to mesoscale results with better time resolution, reducing the traffic emission aggregation from 1-h to minutes.

Multiscale modelling, as the proposed in this paper, seems to be a promising tool to reproduce pollutant dispersion with high resolution in real urban areas. The main added values with respect of using CFD alone are: 1) more accurate information about wind flow properties in the inlet of the CFD numerical domain provided by the coupling with meteorological mesoscale model, which includes information about urban scale processes in the CFD simulation; 2) better resolution in traffic emissions, and thus better modelling of pollutant dispersion. A limitation of this methodology is the detailed information needed (e.g. urban morphology, types of vehicles, position of traffic lights, etc …) to run the three models (mesoscale, emissions and microscale). The computational time of the CFD simulations is not increased respect to using CFD alone and this methodology is portable to other cities and conditions. However, the additional time to run the mesoscale model and emission model should be taken into account. Therefore, this can be useful for policy makers for evaluating microscale population exposure and planning purposes, enabling them to design local abatement measures and exposure assessment taking into account the influences of all relevant scales. However, as shown in the paper, experimental measurements are needed to evaluate the model assumptions and set- up the modelling system, including the selection of turbulent Schmidt number. In future studies, model improvements should be focused on a better representation of several physical processes such as thermal ef- fects, turbulence induced by traffic or coupling between mesoscale and microscale models. In addition, one of the main issues to couple WRF with CFD is linked with the different spatial scales of both models, and in particular the TKE. Then further investigation in the future about how to impose WRF vertical profiles at the inlet of CFD simulations would be recommendable.

Declaration of interest

None.

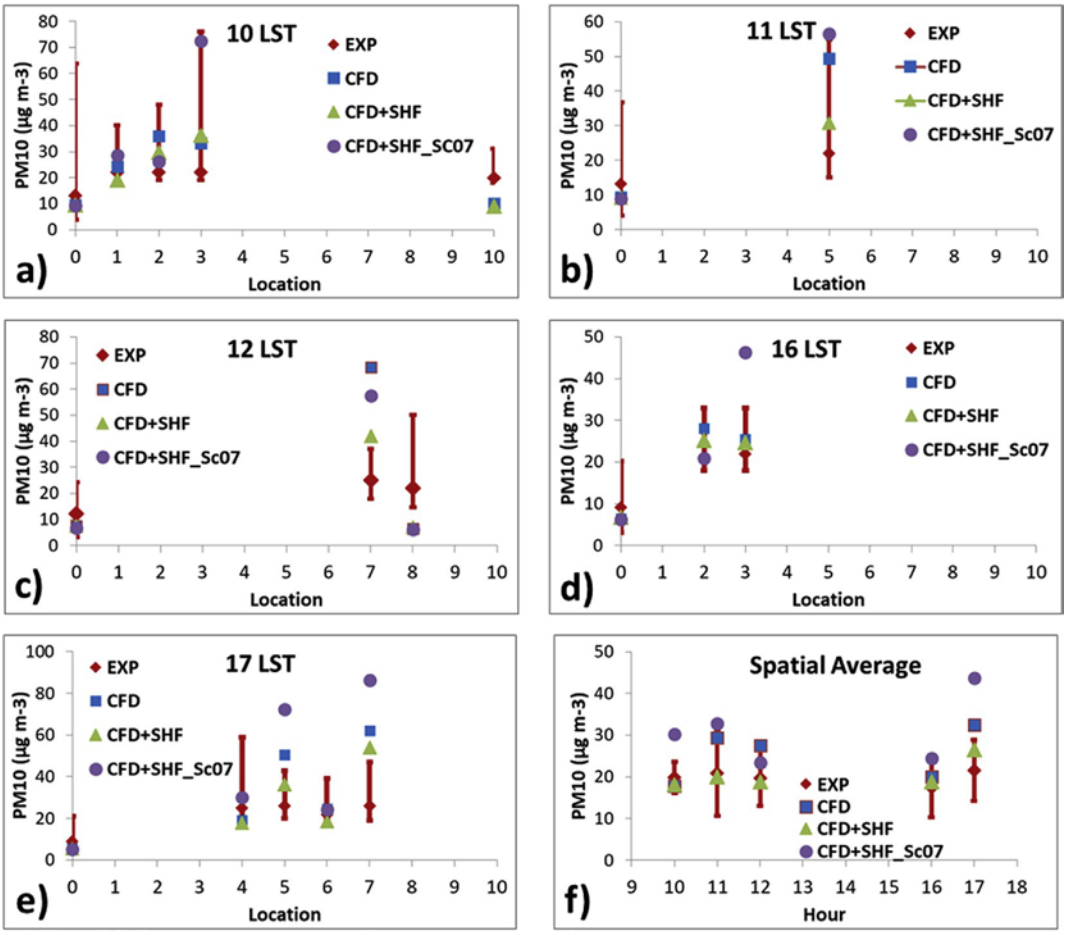

Fig. 11. a) Modelled and measured PM_{10} concentration at 10 LST of 25th February 2015. b), c), d) and e) the same as a) but for 11 LST, 12 LST, 16 LST and 17 LST respectively. Vertical bars represent the range of experimental PM_{10} concentration fluctuations at each position. d) Average concentration over all locations.

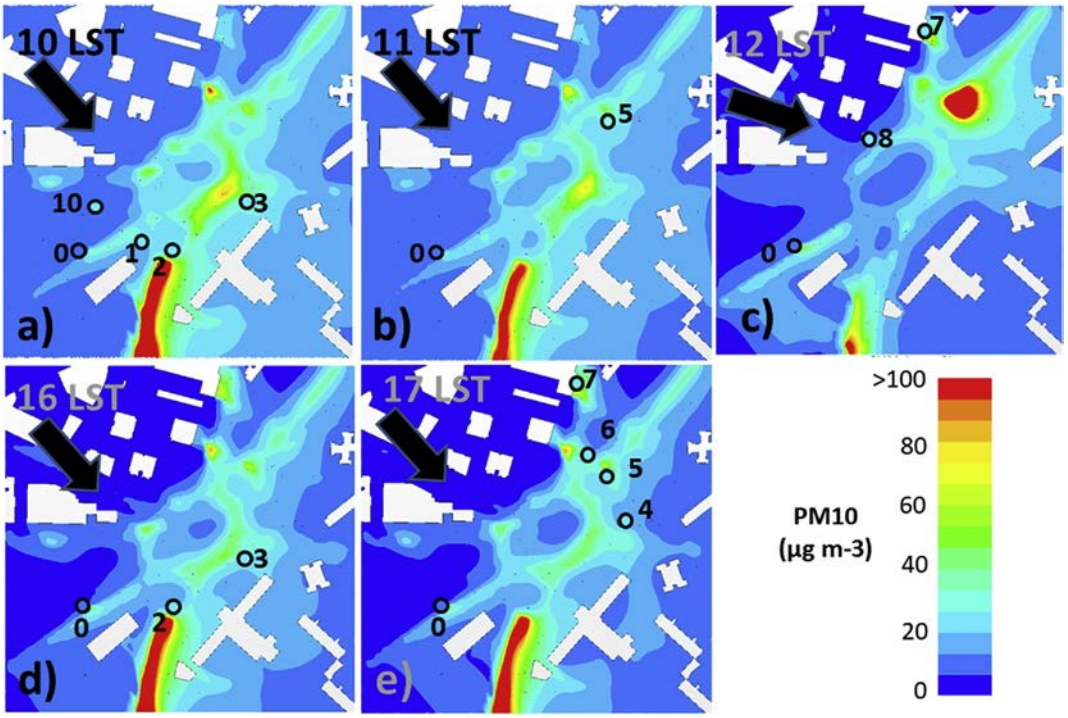

Fig. 12. Modelled PM_{10} concentration considering SHF at ground and S_{ct} = 0.3 at pedestrian level (1.5 m AGL) for 25th February 2015 at a) 10 LST, b) 11 LST, c) 12 LST, d) 16 LST and e) 17 LST. The colour of points indicates the measured concentration at each position and the black arrows represent the inlet wind direction.

Acknowledgements

This study has been supported by the TECNAIRE-CM research pro- ject (S2013/MAE-2972) and AIRTEC-CM (S2018/EMT-4329) funded by The Regional Government of Madrid (Spain). JLS, AM, ER and FM also thank to the support of the RETOS-AIRE (RTI2018-099138-B-I00) project and EXCLUR (CGL2016-80154-R) project funded by the Spanish Ministry of Science, Innovation and Universities. Thanks to Madrid City Council for collaborating in the development of the project. The authors are also grateful to Extremadura Research Center for Advanced Technologies (CETA-CIEMAT) by helping in using its computing facilities for the simulations. CETA-CIEMAT belongs to CIEMAT and the Government of Spain and is funded by the European Regional Development Fund.

References

Abu-Allaban, M., Gillies, J.A., Gertler, A.W., Clayton, R., Proffitt, D., 2003. Tailpipe, re-suspended road dust, and brake-wear emission factors from on-road vehicles. Atmos. Environ. 37, 5283–5293. https://doi.org/10.1016/j.atmosenv.2003.05.005.

Alonso-Estébanez, A., Pascual-Muñoz, P., Yagüe, C., Laina, R., Castro-Fresno, D., 2012. Field experimental study of traffic-induced turbulence on highways. Atmos. Environ. 61, 189–196.

Amato, F., Nava, S., Lucarelli, F., Querol, X., Alastuey, A., Baldasano, J.M., Pandolfi, M., 2010. A comprehensive assessment of PM emissions from paved roads: real-world Emission Factors and intense street cleaning trials. Sci. Total Environ. 408, 4309–4318. https://doi.org/10.1016/j.scitotenv.2010.06.008.

Amorim, J.H., Rodrigues, V., Tavares, R., Valente, J., Borrego, C., 2013. CFD modelling of the aerodynamic effect of trees on urban air pollution dispersion. Sci. Total Environ. 461, 541–551. https://doi.org/10.1016/j.scitotenv.2013.05.031.

Antoniou, N., Montazeri, H., Neophytou, M., Blocken, B., 2019. CFD simulation of urban microclimate: validation using high-resolution field measurements. Sci. Total Environ. 695, 133743. https://doi.org/10.1016/j.scitotenv.2019.133743.

Arrillaga, J.A., Vilà-Guerau de Arellano, J., Bosveld, F., Baltink, H.K., Yagüe, C., Sastre, M., Román-Cascón, C., 2018. Impacts of afternoon and evening sea-breeze fronts on local turbulence, and on CO2 and radon-222 transport. Quart. J. Roy. Meteor. Soc. 144, 990–1011.

Baik, J.-J., Park, S.-B., Kim, J.-J., 2009. Urban flow and dispersion simulation using a CFD model coupled to a mesoscale model. J. Appl. Meteorol. Climatol. 48 (8), 1667–1681. https://doi.org/10.1175/2009JAMC2066.1.

Blocken, B., 2018. LES over RANS in building simulation for outdoor and indoor appli- cations: a foregone conclusion? Build. Simul. 11, 821–870. https://doi.org/10.1007/ s12273-018-0459-3.

Borge, R., Narros, A., Artiñano, B., Yagüe, C., Gomez-Moreno, F.J., de la Paz, D., Roman-Cascon, C., Díaz, E., Maqueda, G., Sastre, M., et al., 2016. Assessment of microscale spatio-temporal variation of air pollution at an urban hotspot in Madrid (Spain) through an extensive field campaign. Atmos. Environ. 140, 432–445. https://doi.org/10.1016/j.atmosenv.2016.06.020.

Borge, R., Santiago, J.L., de la Paz, D., Martín, F., Domingo, J., Valdés, C., Sánchez, B., Rivas, E., Rozas, M.T., Lázaro, S., Pérez, J., Fernández, A., 2018. Application of a short term air quality action plan in Madrid (Spain) under a high-pollution episode - Part II: assessment from multi-scale modelling. Sci. Total Environ. 635, 1574–1584. https://doi.org/10.1016/j.scitotenv.2018.04.323.

Bougeault, P., Lacarrere, P., 1989. Parameterization of orography-induced turbulence in a mesobeta-scale model. Mon. Weather Rev. 117, 1872–1890.

Britter, R., Hanna, S., 2003. Flow and dispersion in urban areas. Annu. Rev. Fluid Mech. 35 (1), 469–496. https://doi.org/10.1146/annurev.fluid.35.101101.161147.

Buccolieri, R., Salim, S.M., Leo, L.S., Di Sabatino, S., Chan, A., Ielpo, P., Gromke, C., 2011. Analysis of local scale tree–atmosphere interaction on pollutant concentration in idealized street canyons and application to a real urban junction. Atmos. Environ. 45, 1702–1713. https://doi.org/10.1016/j.atmosenv.2010.12.058.

Buccolieri, R., Santiago, J.-L., Rivas, E., Sanchez, B., 2018. Review on urban tree modelling in CFD simulations: aerodynamic, deposition and thermal effects. Urban For. Urban Green. 31, 212–220. https://doi.org/10.1016/j.ufug.2018.03.003.

Bukowiecki, N., Lienemann, P., Hill, M., Furger, M., Richard, A., Amato, F., Prévôt, A.S.H., Baltensperger, U., Buchmann, B., Gehrig, R., 2010. PM10 emission factors for non-exhaust particles generated by road traffic in an urban street canyon and along a freeway in Switzerland. Atmos. Environ 44, 2330–2340. https://doi.org/10.1016/J.ATMOSENV.2010.03.039.

Cai, X.M., 2012. Effects of wall heating on flow characteristics in a street canyon. Boundary-Layer Meteorol. 142 (3), 443–467.

Chang, J.C., Hanna, S.R., 2004. Air quality model performance evaluation. Meteorol. Atmos. Phys. 87 (1–3), 167–196. https://doi.org/10.1007/s00703-003-0070-7.

Chen, F., Dudhia, J., 2001. Coupling an advanced land-surface/hydrology model with the Penn State/NCAR MM5 modeling system. Part I: model implementation and sensi- tivity. Monsoon Weather Review 129, 569–585.

Chen, F., Kusaka, H., Bornstein, R., Ching, J., Grimmond, C., Grossman-Clarke, S., Loridan, T., Manning, K.W., Martilli, A., Miao, S., et al., 2011. The integrated wrf/ urban modelling system: development, evaluation, and applications to urban en- vironmental problems. Int. J. Climatol. 31 (2), 273–288. https://doi.org/10.1002/joc.2158.

de la Paz, D., Borge, R., Martilli, A., 2016. Assessment of a high resolution annual WRF-BEP/CMAQ simulation for the urban area of Madrid (Spain). Atmos. Environ. 144, 282–296. https://doi.org/10.1016/j.atmosenv.2016.08.082.

de la Paz, D., Borge, R., Vedrenne, M., Martin, J.L., Amato, F., Karanasiou, A., Boldo, E., Moreno, T., 2015. Implementation of road dust resuspension in air quality simula- tions of particulate matter in Madrid (Spain). Front. Environ. Sci. 3 (72), 1–11. https://doi.org/10.3389/fenvs.2015.00072.

Dejoan, A., Santiago, J.L., Martilli, A., Martín, F., Pinelli, A., 2010. Comparison between Large-eddy simulation and Reynolds-averaged Navier-Stokes computations for the MUST field experiment. Part II: effects of incident wind angle deviation on the mean flow and plume dispersion. Boundary-Layer Meteorol. 135, 133–150. https://doi.org/10.1007/s10546-010-9467-2.

Di Sabatino, S., Buccolieri, R., Olesen, H.R., Ketzel, M., Berkowicz, R., Franke, J., Schatzmann, M., Schlunzen, K., Leitl, B., Britter, R., Borrego, C., Costa, A., Castelli, S., Reisin, T., Hellsten, A., Saloranta, J., Moussiopoulos, N., Barmpas, F., Brzozowski, K., Goricsan, I., Balczo, M., Bartzis, J., Efthimiou, G., Santiago, J., Martilli, A., Piringer, M., Baumann-Stanzer, K., Hirtl, M., Baklanov, A., Nuterman, R., Starchenko, A., 2011. COST 732 in practice: the MUST model evaluation exercise. Int. J. Environ. Pollut. 44, 403–418. https://doi.org/10.1504/IJEP.2011.038442.

Di Sabatino, S., Buccolieri, R., Pulvirenti, B., Britter, R., 2007. Simulations of pollutant dispersion within idealised urban-type geometries with CFD and integral models. Atmos. Environ. 41 (37), 8316–8329. https://doi.org/10.1016/j.atmosenv.2007.06.052.

Eijk, A., Ligterink, N., Inanc, S., 2014. EnViVer 4.0 Pro and Enterprise Manual. TNO & DelfDimensions.

European Environment Agency, 2015. The European Environment State and Outlook 2015: Sythesis Report. EEA, Copenhagen, Denmark, pp. 205. http://www.eea. europa.eu/soer.

European Environment Agency (EEA), 2018. Air Quality in Europe –2018 Report. EEA Technical report no 12/2018 978-92-9213-989-6 Available online at: https://www.eea.europa.eu/publications/air-quality-in-europe-2018.

Ferm, M., Sjöberg, K., 2015. Concentrations and emission factors for PM2.5 and PM10 from road traffic in Sweden. Atmos. Environ. 119, 211–219. https://doi.org/10.1016/j.atmosenv.2015.08.037.

Fontes, T., Pereira, S.R., Fernandes, P., Bandeira, J.M., Coelho, M.C., 2015. How to combine different microsimulation tools to assess the environmental impacts of road traffic? Lessons and directions. Transp. Res. D Transp. Environ. 34, 293–306.

Gehrig, R., Hill, M., Buchmann, B., Imhof, D., Weingartner, E., Baltensperger, U., 2004. Separate determination of PM10 emission factors of road traffic for tailpipe emissions and emissions from abrasion and resuspension processes. Int. J. Environ. Pollut. 22, 312–332. https://doi.org/10.1504/IJEP.2004.005549.

Grimm, H., Eatough, D.J., 2009. Aerosol measurement: the use of optical light scattering for the determination of particulate size distribution, and particulate mass, including the semi-volatile fraction. J. Air Waste Manag. Assoc. 59, 101–107.

Gromke, C., Blocken, B., 2015. Influence of avenue-trees on air quality at the urban neighborhood scale. Part II: traffic pollutant concentrations at pedestrian level. Environ. Pollut. 196, 176–184. https://doi.org/10.1016/j.envpol.2014.10.015.

Gromke, C., Buccolieri, R., Di Sabatino, S., Ruck, B., 2008. Dispersion study in a street canyon with tree planting by means of wind tunnel and numerical investigations - evaluation of CFD data with experimental data. Atmos. Environ. 42, 8640–8650. https://doi.org/10.1016/j.atmosenv.2008.08.019.

Hanna, S., Chang, J., 2012. Acceptance criteria for urban dispersion model evaluation. Meteorol. Atmos. Phys. 116, 133–146. https://doi.org/10.1007/s00703-011-0177-1.

Jeanjean, A., Buccolieri, R., Eddy, J., Monks, P., Leigh, R., 2017. Air quality affected by trees in real street canyons: the case of Marylebone neighbourhood in central London. Urban For Urban Gree 22, 41–53. https://doi.org/10.1007/s00703-011-0177-1.

Ketzel, M., Omstedt, G., Johansson, C., Düring, I., Pohjola, M., Oettl, D., Gidhagen, J., Wåhlin, P., Lohmeyer, A., Haakana, M., Berkowicz, R., 2007. Estimation and vali- dation of PM2.5/PM10 exhaust and non-exhaust emission factors for practical street pollution modeling. Atmos. Environ. 41, 9370–9385. https://10.1016/j.atmosenv. 2007.09.005.

Kwak, K.-H., Baik, J.-J., Ryu, Y.-H., Lee, S.-H., 2015. Urban air quality simulation in a high-rise building area using a cfd model coupled with mesoscale meteorological and chemistry-transport models. Atmos. Environ. 100, 167–177. https://doi.org/10.1016/j.atmosenv.2014.10.059.

Martilli, A., Clappier, A., Rotach, M.W., 2002. An urban surface exchange para- meterization for mesoscale models. Boundary-Layer Meteorol. 104 (2), 261–304. https://doi.org/10.1023/A:1016099921195.

Nazarian, N., Martilli, A., Kleissl, J., 2018. Impacts of realistic urban heating, Part I: spatial variability of mean flow, turbulent exchange and pollutant dispersion. Boundary-Layer Meteorol. 166, 367–393.

Ntziachristos, L., Samaras, Z., 2016. Methodology for the calculation of exhaust emis- sions: SNAPs 070100-070500, NFRs 1A3bi-iv (EMEP/EEA air pollutant emission in- ventory guidebook 2016–update dec. 2016). Available online at: https://www.eea.europa.eu/publications/emep-eea-guidebook-2016/part-b-sectoral-guidance- chapters/1-energy/1-a-combustion/1-a-3-b-i.

Qu, Y., Milliez, M., Musson-Genon, L., Carissimo, B., 2012. Numerical study of the thermal effects of buildings on low-speed airflow taking into account 3D atmospheric radiation in urban canopy. J. Wind Eng. Ind. Aerodyn. 104, 474–483.

Quaassdorff, C., Borge, R., Perez, J., Lumbreras, J., de la Paz, D., de Andres, J.M., 2016. Microscale traffic simulation and emission estimation in a heavily trafficked round- about in Madrid (Spain). Sci. Total Environ. 566, 416–427. https://doi.org/10.1016/j.scitotenv.2016.05.051.

Richards, P.J., Hoxey, R.P., 1993. Appropriate boundary conditions for computational wind engineering models using the k-ε turbulence model. J. Wind Eng. Ind. Aerodyn.

46, 145–153.
Rivas, E., Santiago, J.L., Lechón, Y., Martín, F., Ariño, A., Pons, J.J., Santamaría, J.M., 2019. CFD modelling of air quality in Pamplona City (Spain): assessment, stations spatial representativeness and health impacts valuation. Sci. Total Environ. 649, 1362–1380. https://doi.org/10.1016/j.scitotenv.2018.08.315.
Salamanca, F., Krpo, A., Martilli, A., Clappier, A., 2010. A new building energy model coupled with an urban canopy parameterization for urban climate simulations-part I. formulation, verification, and sensitivity analysis of the model. Theor. Appl. Climatol. 99 (3–4), 331–344. https://doi.org/10.1007/s00704-009-0142-9.
Sanchez, B., Santiago, J.L., Martilli, A., Martin, F., Borge, R., Quaassdorff, C., de la Paz, D., 2017. Modelling NOx concentrations through CFD-RANS in an urban hot-spot using high resolution traffic emissions and meteorology from a mesoscale model. Atmos. Environ. 163, 155–165. https://doi.org/10.1016/j.atmosenv.2017.05.022.
Santiago, J.L., Borge, R., Martin, F., de la Paz, D., Martilli, A., Lumbreras, J., Sanchez, B., 2017a. Evaluation of a CFD-based approach to estimate pollutant distribution within a real urban canopy by means of passive samplers. Sci. Total Environ. 576, 46–58. https://doi.org/10.1016/j.scitotenv.2016.09.234.
Santiago, J.L., Buccolieri, R., Rivas, E., Calvete-Sogo, H., Sanchez, B., Martilli, A., Alonso, R., Elustondo, D., Santamaría, J.M., Martín, F., 2019. CFD modelling of vegetation barrier effects on the reduction of traffic-related pollutant concentration in an avenue of Pamplona, Spain. Sustain. Cities Soc. 48, 101559. https://doi.org/10.1016/j.scs. 2019.101559.
Santiago, J.L., Dejoan, A., Martilli, A., Martín, F., Pinelli, A., 2010. Comparison between Large-eddy simulation and Reynolds-averaged Navier-Stokes computations for the MUST field experiment. Part I: study of the flow for an incident wind directed per- pendicularly to the front array of containers. Boundary-Layer Meteorol. 135, 109–132. https://doi.org/10.1007/s10546-010-9466-3.
Santiago, J.L., Krayenhoff, E.S., Martilli, A., 2014. Flow simulations for simplified urban configurations with microscale distributions of surface thermal forcing. Urban Clim. 9, 115–133. https://doi.org/10.1016/j.uclim.2014.07.008.
Santiago, J.-L., Martilli, A., Martin, F., 2017b. On dry deposition modelling of atmo- spheric pollutants on vegetation at the microscale: application to the impact of street vegetation on air quality. Boundary-Layer Meteorol. 162, 451–474. https://doi.org/ 10.1007/s10546-016-0210-5.
Santiago, J.L., Martín, F., Martilli, A., 2013. A computational fluid dynamic modelling approach to assess the representativeness of urban monitoring stations. Sci. Total Environ. 454–455, 61–72. https://doi.org/10.1016/j.scitotenv.2013.02.068.
Santiago, J.-L., Rivas, E., Sanchez, B., Buccolieri, R., Martin, F., 2017c. The impact of planting trees on NOx concentrations: the case of the plaza de la Cruz neighborhood in pamplona (Spain). Atmosphere 8, 131. https://doi.org/10.3390/atmos8070131.
Schatzmann, M., Olesen, H., Franke, J., 2010. COST 732 Model Evaluation Case Studies: Approach and Results. Distributed by University of Hamburg (Germany), Meteorological Institute, Hamburg, Germany3-00-018312-4 2007.
Sini, J.F., Anquetin, S., Mestayer, P.G., 1996. Pollution dispersion and thermal effects in urban street canyon. Atmos. Environ. 30, 2659–2677. https://doi.org/10.1016/ 1352-2310(95)00321-5.
Skamarock, W.C., Klemp, J.B., 2008. A time-split nonhydrostatic atmospheric model for weather research and forecasting applications. J. Comput. Phys. 227, 3465–3485. https://doi.org/10.1016/j.jcp.2007.01.037.
Smit, R., McBroom, J., 2009. Development of a new high-resolution traffic emissions and fuel consumption model. Road Transp. Res. 18 (4), 3–13.
Smit, R., Smokers, R., Rabe, E., 2007. A new modelling approach for road traffic emis- sions: VERSIT+. Transp. Res. D Transp. Environ. 12 (6), 414–422. https://doi.org/10.1016/j.trd.2007.05.001.
Solazzo, E., Cai, X., Vardoulakis, S., 2008. Modelling wind flow and vehicle-induced turbulence in urban streets. Atmos. Environ. 42, 4918–4931.
Tasic, V., Jovasevic-Stojanovic, M., Vardoulakis, S., Milosevic, N., Kovacevic, R., Petrovic, J., 2012. Comparative assessment of a real-time particle monitor against the re- ference gravimetric method for PM 10 and PM 2.5 in indoor air. Atmos. Environ. 54, 358–364.
Tominaga, Y., Stathopoulos, T., 2007. Turbulent Schmidt numbers for CFD analysis with various types of flow field. Atmos. Environ. 41 (37), 8091–8099. https://doi.org/10.1016/j.atmosenv.2007.06.054.
Toparlar, Y., Blocken, B., Vos, P., Van Heijst, G.J.F., Janssen, W.D., van Hooff, T., Montazeri, H., Timmermans, H.J.P., 2015. CFD simulation and validation of urban microclimate: a case study for Bergpolder Zuid, Rotterdam. Build. Environ 83, 79–90. https://doi.org/10.1016/j.buildenv.2014.08.004.
Toparlar, Y., Blocken, B., Maiheu, B., van Heijst, G.J.F., 2017. A review on the CFD analysis of urban microclimate. Renew. Sustain. Energy Rev. 80, 1613–1640. https://doi.org/10.1016/j.rser.2017.05.248.
Vardoulakis, S., Fisher, B.E.A., Pericleous, K., Gonzalez-Flesca, N., 2003. Modelling air quality in street canyons: a review. Atmos. Environ. 37, 155–182.
Vardoulakis, S., Dimitrova, R., Richards, K., Hamlyn, D., Camilleri, G., Weeks, M., Sini, J.- F., Britter, R., Borrego, C., Schatzmann, M., Moussiopoulos, N., 2011. Numerical model inter-comparison for wind flow and turbulence around single block buildings. Environ. Model. Assess. 16, 169–181.
Vranckx, S., Vos, P., Maiheu, B., Janssen, S., 2015. Impact of trees on pollutant dispersion in street canyons: a numerical study of the annual average effects in Antwerp, Belgium. Sci. Total Environ. 532, 474–483. https://doi.org/10.1016/j.scitotenv. 2015.06.032.
World Health Organiztion (WHO), 2018. Ambient (outdoor) air quality and health. Fact sheet, Updated May 2018. Available online at: https://www.who.int/news-room/ fact-sheets/detail/ambient-(outdoor)-air-quality-and-health.
Xie, X., Liu, C.H., Leung, D.Y.C., 2007. Impact of building facades and ground heating on wind flow and pollutant transport in street canyons. Atmos. Environ. 41, 9030–9049. Yaghoobian, N., Kleissl, J., 2012. An indoor-outdoor building energy simulator to study urban modification effects on building energy use-model description and validation. Energy Build. 54, 407–417.